Available online at www.sciencedirect.com
SCIENCE DIRECT®
International Journal of Heat and Mass Transfer 48 (2005) 5221–5239
International Journal of HEAT and MASS TRANSFER
www.elsevier.com/locate/ijhmt

Evaluation of flame emission models combined with the discrete transfer method for combustion system simulation

P.S. Cumber [a,*], M. Fairweather [b]

[a] School of Engineering and Physical Science, Heriot-Watt University, Edinburgh EH14 4AS, UK
[b] Energy and Resources Research Institute, School of Process, Environmental and Materials Engineering, University of Leeds, Leeds LS2 9JT, UK

Received 15 October 2004
Available online 3 October 2005

Abstract

This article considers the application of flame emission models used for predicting the thermal radiation fluxes from flames and fires within a computational fluid dynamic framework, used in conjunction with the discrete transfer method. The flame emission models differ in their generality, sophistication, accuracy and computational cost, and are assessed in terms of their ability to predict radiation transfer in idealised situations, as well as flames in tubes representative of burner systems, laboratory-scale jet flames and wind-blown jet fires. It is concluded that the implementation of simple flame emission models, based on the grey gas assumption, must be treated with caution due to convergence problems. The key problem occurs when the grey absorption coefficient is based on a length scale linked to the size of the control volume. This issue is well known in the radiation modelling community, but not so in the combustion modelling community. Use of models based on the banded mixed grey gas, TTNH, wide and narrow band approaches yield satisfactory results for all the simulated flames and fires considered, typically being within 20% of the measured radiation heat flux.

Keywords: Radiation heat transfer; Flame emission models; Discrete transfer method; Fire modelling; Combustion systems

1. Introduction

The mathematical modelling of high temperature processes requires an ability to predict the thermal radiation fields with confidence. The fundamental quantity of interest, the spectral intensity, depends in a complex way on the temperature and participating species distributions. This, together with the fact that the spectral intensity is a function of location, orientation and wavelength, makes the simulation of combusting flows a challenging scientific computation. Even with today's computer hardware and the routine use of parallel computing facilities choices have to be made regarding the balance between the levels of sophistication of the radiation model relative to other sub-models that form the composite flame or fire model. In this article a number of radiation models are evaluated with respect to their accuracy and suitability to be combined with a computational fluid dynamic (CFD) model for simulating a number of idealised and generic flows.

* Corresponding author. Tel.: +44 131 451 3532; fax: +44 131 451 3129.
E-mail address: p.s.cumber@hw.ac.uk (P.S. Cumber).

0017-9310/$ - see front matter © 2005 Elsevier Ltd. All rights reserved.
doi:10.1016/j.ijheatmasstransfer.2005.07.032

Nomenclature

$a_{i,j,1}$, $a_{i,j,2}$	coefficients in the mixed grey gas model
f_v	soot volume fraction
I	spectrally integrated intensity
$I_{b,v}$	black body spectral intensity
k	wall thermal conductivity
K_a	grey gas absorption coefficient
l	path length
n	number of control volumes
N_φ	number of rays in the φ direction
N_θ	number of rays in the θ direction
N_{Ray}	number of rays
N_g	number of grey gases for gas emission in the mixed grey gas model
N_s	number of grey gases for soot emission in the mixed grey gas model
q	heat flux
q_{tot}	total heat flux
q_{CD}	conduction heat flux through wall
q_{CV}	convection heat flux to wall
q_R	radiation heat flux
r	radial distance
S	speed-up factor
S_{CV}	speed-up factor per control volume
S_{Ray}	speed-up factor per ray
S/d	mean line intensity to line spacing ratio
T	temperature
T_{water}	cooling water temperature
x	downwind distance or axial distance
X_j	partial density path length of species j

Greek symbols

α	integrated band intensity
Δs	path length through a homogeneous volume
Δ_w	wall thickness
ε_T	total emissivity
ε_w	wall emissivity
η	line width to spacing ratio
φ	angle of rotation
v	wave number
v_u	upper limit on a wide band
θ	angle of incidence
ρ	partial density
σ	Stefan Boltzmann constant
τ	transmittance
τ_H	optical depth at band head
ω	band width parameter

Subscripts

$-$	property incident to a wall
$+$	property emitted from wall
g	gas phase property
i	spectral band
i,j	ray indices
j	gaseous species
$n, n-1$	exit and entry points of ray traversing a volume
v	spectral property
s	property of soot
w	wall property

Example areas of application are as part of mathematical models used in the safety analysis of high-pressure plant and pollution control in heating plant. The safe design and operation of high-pressure plant and pipe work requires that provision be made for the relief of pressure under certain operational and emergency conditions. The consequences of a release must also be evaluated so that appropriate safety measures can be adopted during the relief process. In addition, assessments of the consequences associated with accidental releases of flammable material are required as the basis of safety reports and risk assessments on existing and proposed installations. For flammable gases and vapours it is necessary to be able to predict the thermal radiation fluxes that any fire might impose on its surroundings—either by direct flame impingement of the fire on an item of plant or at distance from the fire by radiation transmitted through the atmosphere. This information is in turn used to provide estimates, for example, of vessel survival times, building burning distances and escape times for personnel.

In addition to the safety analysis of fires, increasing concerns over the environmental impact of heating plant such as boilers and furnaces requires that the energy balance during their operation is evaluated accurately. Insight into the energy transfer processes of heating plant is necessary to ensure that the temperature sensitive reaction rates relevant to pollution production, such as NO_x and SO_x, can be estimated. In this way it is possible to predict pollution concentrations such that they can be assessed and minimised by good design.

Radiation heat transfer in fires and flame tubes differs significantly in a number of ways. For the natural gas combustion processes considered in the present work, the thermal radiation field in a jet fire, for example, is highly anisotropic with significant levels of radiation in discrete spectral windows determined by the emitting species present in the combustion products and fuel. In an enclosed flame such as that present in a flame tube the radiation field is more isotropic and if significant levels of soot are present then the spectral radiation has a more continuous distribution in wave number space.

However, for both types of flame a number of modelling issues are common, such as the flame structure used as input to the radiation model. Predictions of the structure of fires using either integral [1] or numerical [2] techniques require that some representation be made of the absorption and emission characteristics of the products of combustion to allow solution of the radiation transfer equation. In particular, flame emission models are required for the gaseous species and unburned carbon particulates that occur within the fire. As an example, recent experimental and theoretical work [2] which considered a number of jet fires (up to 2.7 GW in size) stabilised on subsonic releases of natural gas demonstrated that the contribution from soot particles to total radiation fluxes measured about these fires was at most 40% and likely to be much less than this. In the case of sonic natural gas jet fires the residence time is sufficiently small for soot production to be significantly reduced as insufficient time is available for the particles of soot to form before being advected out of the high temperature region of the fire [3]. The visible flame envelope for sonic natural gas jet fires has a bluish colour, suggesting that the contribution of emissions from soot particles to the total radiation flux is insignificant.

This article considers the application of a number of flame emission models to predict the radiation fluxes from jet fires and within flame tubes. Each flame emission model is applied in conjunction with the discrete transfer method [4] for solving the equation of radiation transfer where appropriate or a discretisation of the radiation heat transfer equation in its integral form. All implementations use a numerical quadrature to evaluate the incident radiation flux integral and in that respect they are similar to the discrete transfer method. The discrete transfer method has been adopted due to its frequent use in fire modelling codes, as well as its computational economy, ease of implementation and conceptual simplicity [4], although in its original form there are issues relating to the accuracy of the radiation source field [5]. However, some of the conclusions drawn are independent of the radiation solution algorithm implemented and can therefore be considered equally relevant to the discrete-ordinates method, the finite-volume method and the Monte Carlo method, and these issues will be considered further in later sections.

The flame emission models considered differ in their generality, sophistication, accuracy and computational cost, and are each assessed in terms of their ability to predict radiation transfer from one-dimensional idealised representations of the internal structure of non-premixed flames, as well as from laboratory and field-scale jet fires and flame tube simulations. Of particular interest is the accuracy and computational cost of the various modelling approaches and their suitability for application in combination with a CFD model to predict the flow fields. The present work considers the appropriate choice of flame emission model to achieve the optimum balance between model accuracy and computational cost. An additional interest is how the degree of inhomogeneity and soot level influences a flame emission model's accuracy and generality. Whilst this might be expected to be the case, the question of quantification remains.

2. Radiation heat transfer models

Many thermal radiation models have been developed in the past, usually with a specific application area in mind. For example, the mixed grey gas model, or the weighted sum of grey gas model, were originally formulated for hand calculations of gas emissivities and have been successfully applied to zone models of furnaces [6]. More recently mixed grey gas models have been used as part of CFD models to predict flashover [7], flame spread [8] and furnace performance [9]. Trivic [9] showed that the radiation source term in a furnace could be calculated with accuracy provided a sufficient number of grey gases are used. Soufiani and Djavdan [10] completed a similar exercise but only considered the weighted sum of grey gases with 3 grey gases and 1 clear gas. Soufiani and Djavdan reported significant errors in wall fluxes and volumetric source terms especially when significant temperature variations exist. For the test cases they considered, these authors also reported a speed-up of 50 times when using a weighted sum of grey gases approach compared to a narrow band model, a value in direct proportion to the nominal partition of spectral space, i.e. 4 grey gases to 200 narrow bands.

Narrow band models were originally formulated for studying atmospheric physics and latterly have been used to evaluate the radiation field surrounding jet fires where the flame structure was calculated by a CFD model [2,3,11]. The computational cost of a narrow band model tends to restrict its application to fire simulation where the flow fields are converged and the radiation fields calculated as a post-process. In these simulations the radiation loss to the energy budget is therefore accounted for in a simple way. The wide band model of Edwards et al. [12–14], based on the grey band assumption, although not restricted to a specific area of application was formulated for ease of calculation and not for integration within a CFD framework. It has been found that the spectral form of the wide band model is more suited to CFD calculations [15], although the spectral integration must be evaluated numerically rather than directly (as is possible with the grey band representation). The spectral band parameters have been calibrated [14] for application with the grey band representation.

In previous studies narrow and wide band models have been compared for simplified one- and two-dimensional

idealised cases. Marakis [16] applied two narrow band models, RADCAL and a narrow band model based on an exponential tailed line-intensity distribution [17], as well as Edwards et al. exponential wide band model [12–14]. These models were applied to planar bench mark problems solved by Kim et al. [18] using the S–N discrete-ordinates method with the S_{20} quadrature scheme. For non-homogeneous planar systems Marakis used wide band scaling [14] and found this improved the agreement with Kim et al.'s benchmark solutions, but the computational cost was significant. Wide band scaling was considered further by Strohle and Coelho [19] who applied a number of different implementations of the exponential wide band model to calculate radiation heat transfer in one- and two-dimensional enclosures. For the implementations considered, Strohle and Coello concluded that the wide band correlated k-distribution method provided the optimal balance between accuracy and computational effort. For the most part independent validation or evaluation of radiation models where a range of models are compared against each other for a range of test cases is limited. The exception to this is Lallemant et al. [20] review article which included an analysis of a number of total emissivity models and correlations for homogeneous systems and real combustion systems. Lallemant et al. [20] also considered the application of spectral models such as Edward's exponential wide band model. Lallement et al. [20] differs from the present article in that they used a furnace experiment to evaluate the suitability of a number of flame emission models using the measurements of temperature and participating species as input to the radiation models. The furnace they considered was an experimental furnace located at the Burner Engineering Research Laboratory at the Livermore Laboratories. The flow fields are non-homogeneous but the gradients in the temperature and participating species fields are significantly less than occur in a free jet fire. Therefore no systematic evaluation of these radiation models exist where the flow fields have been calculated as part of a CFD simulation in the open literature, particularly for realistic three-dimensional problems with large gradients in the temperature and participating species fields.

2.1. Flame emission models—participating species

The flame emission models employed in the present work are:

- a grey gas approach using total emissivity curve fits derived by Modak [21],
- a mixed grey gas model developed by Truelove [6],
- a banded implementation of Truelove's [6] mixed grey gas model,
- the total transmittance, non-homogeneous (TTNH) model of Grosshandler [22],
- a spectral version of the exponential wide band model developed by Edwards and Balakrishnan [13], and
- a statistical narrow band model, RADCAL, developed by Grosshandler [22].

The flame emission models listed above are of interest as they are established models that can be considered typical of their respective type. For example, Lallement et al. [20] describe Trueloves mixed grey gas model as being representative of the weighted sum of grey gas models. In addition they are all relatively easy for a practicing combustion engineer to implement or the model is available as open software. It should be noted as discussed above that there is an accepted hierarchy of generality and accuracy within the list of models, with the narrow band model being the most general and accurate; similarly there is an accepted hierarchy of simplicity with the grey gas approach being the most simple to implement. The precise model a combustion engineer should use to predict the radiation field is dependent on the application and the degree of accuracy required. In many situations the appropriate choice is a balance between the most accurate and the most computationally frugal. For all models considered the original developers' model calibration has been used rather than recalibrating each model against a consistent set of experimental or theoretical data, similar to the Lallement et al. [20] study, although it is recognised that a model recalibration has been used in other studies [10]. This decision was taken as the original calibration of the models is a component of the model and any conclusions drawn are immediately applicable to model implementations already in use by the combustion modelling community.

Modak's [21] method is a simple and accurate technique for computing the emissivities and absorptivities of isothermal, homogeneous mixtures of CO_2 and H_2O based on curve fits to emissivities using a wide band model to provide the emissivities in the curve fitting process. The technique was later extended to include CO and CH_4 [23]. In a grey gas approach the total emissivity is calculated from Modak's emissivity curve fits and a grey absorption coefficient is evaluated by inverting the relation

$$\varepsilon_T = 1 - e^{-K_a \Delta s} \tag{1}$$

given a length scale or a partition of a ray, Δs.

The mixed grey gas model of Truelove [6] is based on representing the banded spectra of CO_2 and H_2O as a mixture of clear and grey gases, with the clear component corresponding to the non-emitting regions of the spectrum between strong gas bands. The calculations reported below employ the four-term, one clear and three grey gas expansions fitted by Truelove [6] to gas mixture

total emittance (for the combined emissions of CO_2 and H_2O) evaluated from spectral data. Extensions of this method, described by Truelove [6], to incorporate CO and CH_4 emissions, were also implemented in the present work, and calculations were performed using fits based on a partial pressure ratio typical for natural gas combustion. It is also possible to implement the mixed grey gas method in a banded form [24] where, for a given model spectrum, the grey gas weightings are determined as black body fractional functions for specific sub-line spectral regions. The method employed again used a one clear and three grey gas representation, with the weighting functions taken from Truelove [6]. This will be considered further below in the context of soot emission modelling.

The TTNH model [22,23] is based on total transmittance data for homogeneous gases, with effective partial pressure-path lengths and temperatures for non-homogeneous systems taken as gas concentration weighted averages along a line-of-sight. The starting point for the TTNH model is the fundamental equation for radiation heat transfer in its integral form, ignoring scattering

$$I_{\mathrm{w},-} = \int_0^{\infty} I_{v,\mathrm{w},+}\tau_v(l) - \int_1^{\tau_v(l)} I_{b,v}\,\mathrm{d}\tau_v\,\mathrm{d}v \qquad \tau_v = \mathrm{e}^{-\int_0^x \sum_i \rho_i K_{\mathrm{a},v,i}\,\mathrm{d}x} \tag{2}$$

where $I_{w,-}$ is the intensity incident on a surface and for simplicity the emissivity of the emitting surface is taken to be black. Representing the non-homogenous path as a series of homogeneous elements and using the total transmittance approximation for the integrated spectral emission, the integral equation takes the form

$$I_{\mathrm{w},-} = I_{\mathrm{w},+}\bar{\tau}_{\mathrm{g},n} + \frac{\sigma}{\pi}\sum_{i=1}^{n} T_i^4\left(\bar{\tau}_{\mathrm{g},i-1} - \bar{\tau}_{\mathrm{g},i}\right) \tag{3}$$

where the overbar indicates an effective transmittance evaluated using weighted average temperatures and partial pressures. Thus all spectral integrations are avoided as the total transmittances can be evaluated using any convenient correlation, such as Modak's emissivity curve fits. The temperature correction factor to the transmittance suggested by Grosshandler [22] was not considered in detail in the present work due to its limited range of applicability, although its use is considered further below. Originally the TTNH model was formulated for CO_2 and H_2O mixtures [22,25] and was later extended to include CO and CH_4 [23] by extending Modak's emissivity curve fits. More details of the TTNH model can be found in [22,23,25].

The spectral version of the exponential wide band model developed by Edwards et al. [12–14], described in detail by Edwards [14], is based on the assumption that absorption and emission of radiation by a molecular gas is concentrated in between one and six wide vibrational bands. Within these bands, the spectral lines associated with rotational modes of energy storage are re-ordered in wave number space with exponentially decreasing line intensities moving away from the band head. The band shape is then approximated by one of three simple exponential functions, with the radiation properties of each absorption band obtained from specified model parameters calibrated with experimental measurements

$$\tau_{\mathrm{g},v} = \exp\left(-\sum_{i,j}\frac{\left(\frac{S}{d}\right)_i X_j}{\left(1+\left(\frac{S}{d}\right)_i\left(\frac{X}{\eta}\right)_j\right)^{1/2}}\right) \qquad \left(\frac{S}{d}\right)_i = \left(\frac{\alpha}{\omega}\right)\mathrm{e}^{-\frac{(v_{\mathrm{u}}-v)}{\omega}} \tag{4}$$

where i denotes a particular spectral band and j denotes a participating species. The functionality specified for the mean line intensity to spectral line spacing ratio, $(S/d)_i$, is for an asymmetric band with an upper limit v_{u}. Band overlap is also taken into account for multiple bands and mixtures of gases. The version of this model implemented accounts for mixtures of CH_4, CO, CO_2 and H_2O.

Lastly, the narrow band model of Grosshandler [22], RADCAL is based on the Goody statistical model [26] with equal line strengths within each narrow band region and with non-homogeneous effects accounted for through the Curtis–Godson approximation [25], a narrow band scaling technique.

2.2. Flame emission models—soot

In the combustion system simulations considered later, where soot emission is a major component in the energy transfer balance, significant concentrations of soot modify the spectral intensity distribution and the effect of soot is included in each of the flame radiation models in a manner consistent with emission from the participating gas species.

The mixed grey gas model including emission from soot includes two grey gases for soot as discussed by Truelove [6]. The mixed grey gas model in its banded form including soot is

$$\tau_{i,j}(\Delta s) = \mathrm{e}^{-(K_{\mathrm{g},i}P_{\mathrm{g},i}+K_{\mathrm{s},j}f_{\mathrm{v}})\Delta s}$$
$$I_{n+1,i,j} = (1-\tau_{i,j})a_{i,j}(T_c)\frac{\sigma T_c^4}{\pi} + \tau_{i,j}I_{n,i,j} \tag{5}$$
$$a_{i,j} = a_{i,j,1} + a_{i,j,2}T, \quad \sum_{i=1}^{N_{\mathrm{g}}}\sum_{j=1}^{N_{\mathrm{s}}} a_{i,j}(T) = 1$$

This effectively makes the mixed grey gas model an eight-banded model. Further details of the mixed grey gas model may be found elsewhere [24].

The TTNH model is modified to include soot emission by extending the recurrence relation (3) applied along rays to calculate the incident intensity to

$$I_{w,-} = I_{w,+}\bar{\tau}_{g,n}\tau_{s,n} + \frac{\sigma}{\pi}\sum_{i=1}^{n} T_i^4(\bar{\tau}_{g,i-1}\tau_{s,i-1} - \bar{\tau}_{g,i}\tau_{s,i}) \quad (6)$$

where the soot transmittance, τ_s is evaluated using local temperatures and hence by convention does not have an overbar.

Lastly in the narrow and wide band models the spectral soot transmissivity takes the form,

$$\tau_{s,v} = e^{-Cf_v vl} \quad (7)$$

and the spectral transmittance including emission from the participating species and soot is,

$$\tau_v = \tau_{s,v}\tau_{g,v} \quad (8)$$

The constant C in the soot transmittance equation (7) takes the value of 7, as suggested by Dalzell and Sarofim [27].

All the models employed were implemented in their standard form and precisely as described by the various authors noted above. Although numerous techniques are available to improve the range of applicability, accuracy and computer run-time of many of these methods, these were not pursued in order to ensure a base-line comparison of the various approaches, and to simulate the way in which most researchers use these models. However, the conclusions with respect to run-time and accuracy of the various flame emission models given here for the 'standard' implementation can be factored into any novel implementations of the models. For example, Yan and Holmstedt [28] managed to speed up the narrow band model RADCAL by performing a 'once and for all' evaluation of the line strength to line spacing parameter and strong line parameter for a set of temperatures and wave numbers for CO_2 and H_2O and using a look up table during a simulation. Yan and Holmstedt report a speed-up of 20 times with a difference in prediction of less than 1% compared to the original implementation.

3. Discrete transfer method and non-homogeneous systems

For all of the simulations considered below numerical solutions to the equation of radiation heat transfer were derived using the discrete transfer method [4], or a discrete analogue of the radiation heat transfer equation expressed in its integral form. In its original formulation, the discrete transfer method expresses the transfer equation in a form applicable to homogeneous and grey media. The latter equation is then used to derive a recurrence relation which is applied repeatedly along a ray passing through the homogeneous control volumes defined by the numerical solution procedure for the fluid dynamic equations. By applying this relation to each control volume in turn, inhomogeneities in the overall flow field are accounted for and the total intensity of radiation incident at the end point of the ray determined. The net radiation flux at a given point is then obtained by repeating this calculation for a number of representative rays which are all incident at that point. Extension of this method to non-grey systems using the mixed grey gas approach and applying the recurrence relation over a number of wavelength bands has been described by Lockwood and Shah [4]. Further extensions to allow the incorporation of the spectral version of the wide band model have been described by Cumber et al. [15]. This approach avoids the use of scaling techniques necessary when a discrete form of the fundamental equation for radiation heat transfer is used in its integral form. This makes the discrete transfer method computationally frugal but requires the assumption that the spectral intensity averaged over a wave band interval,

$$\bar{I}_v = \frac{1}{\Delta v}\int_{\Delta v} I_v \, dv \quad (9)$$

and the band averaged spectral absorption coefficient,

$$\overline{K_{a,v}I_v} = \overline{K}_{a,v}\bar{I}_v \quad (10)$$

are uncorrelated (10). This assumption cannot always be justified. Okamoto et al. [29] have explored this issue in the context of a narrow band model and identified the line overlap parameter as key to identifying when the intensity and absorption coefficient are uncorrelated. Cumber et al. [15] and other research groups have shown that for methane jet fires over a range of physical scales using a wide band model with this approach yields satisfactory results. Strohle and Coelho [19] reported significantly better accuracy for a number of idealised test cases when a wide band scaling technique was implemented rather than invoking the uncorrelated band averaged intensity and absorption coefficient assumption. However, the improved accuracy came with an increase in computer run-time of between three and four orders of magnitude.

In obtaining the results described below the discrete transfer method was used either in conjunction with specified gas temperature and species profiles, or with local values of the latter parameters and path lengths determined from solutions to the fluid flow equations. For each combustion system simulation the specific formulation of the numerical model will be considered in turn.

4. Test cases

Four scenarios were used to evaluate the radiation heat transfer models described below, an idealised one-

dimensional non-homogeneous system, an axisymmetric flame tube simulation, a laboratory-scale free jet flame and a sonic field-scale jet fire in a cross-wind. The one-dimensional idealised case is included as a starting point in the comparison exercise and is typical of the type of test problem considered in previous radiation model comparison exercises. The remaining three are combustion system simulations that range from relatively homogeneous isotropic high temperature systems at moderate scale to highly non-homogeneous anisotropic systems at small and large-scale. The combustion systems also have a variation in their tendency to produce soot and thereby also make it possible to assess the importance of banded emission from participating species and continuous emission from soot particles.

In each of the combustion system simulations the mathematical and numerical basis is appropriate for the particular situation and will be described in each case. As well as the reasons given above the combustion systems were chosen as experimental measurements of radiation heat flux distributions and details of the experimental set up are available in the open literature.

4.1. Idealised one-dimensional test case

The idealised one-dimensional test case is representative of the non-homogeneous paths encountered in flames and fires. Fig. 1 shows temperature and mass fraction profiles for a path similar to that considered by Grosshandler [22]. These profiles may be considered representative of the radial temperature and concentration distributions that are found downstream of a burner in a flame tube or the source of a jet fire.

4.2. Flame tube

The geometry of the flame tube is given in Fig. 2. The flame tube consists of a burner section followed by a cylindrical furnace section with water cooled walls. The fuel is natural gas with a co-flow of air. The mass

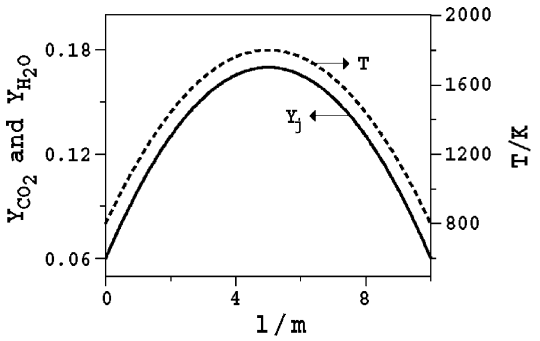

Fig. 1. Temperature and composition distributions for the one-dimensional test case.

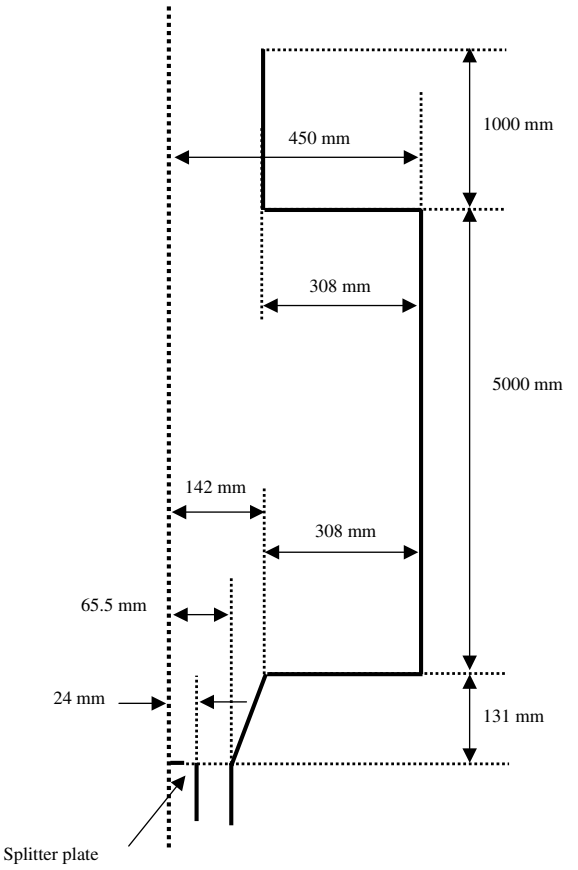

Fig. 2. Wu and Fricker's flame tube geometry.

flow rate of the natural gas is 100 kg h^{-1}, equivalent to a power input of 1.1 MW. The airflow rate is sufficient to give stoichiometric conditions under perfect mixing. Further details of the experiment can be found in [30].

4.3. Laboratory-scale jet flame

The laboratory-scale flame considered here was reported by Baillie et al. [31] and was stabilised on a release of methane issuing vertically from an 8.6 mm internal diameter circular pipe at a mean exit velocity of 20 m s^{-1}. A second concentric pipe of 23 mm diameter was also employed so that a small co-flow of methane through the annular gap between the two pipes could be used to stabilise the main flame. The resulting flame was 1.1–1.2 m in height.

4.4. Field-scale jet fire in a cross-wind

The last test case is a field-scale fire [32] formed by a vertical, moderately underexpanded sonic release of natural gas at 65.1 kg s^{-1} from a 16.2 m high, 385 mm internal diameter, circular pipe. This fire, which was

approximately 60 m in length, was subjected to a cross-wind with a velocity at 9 m above ground level of 6.4 m s^{-1}.

5. Fluid flow and heat transfer models

In this section the different flow models and details of the numerical methodology for each combustion system simulation is presented.

5.1. Flame tube simulation

The geometry of the flame tube is axisymmetric. The mathematical basis of the flow model used in each of the simulations is similar reflecting the turbulent character of each flow. For the flame tube the mathematical basis of the flow model is now considered. The mean flow fields were calculated using the averaged forms of the density-weighted transport equations, with closure achieved using a standard k–ε turbulence model. To account for the influence of the furnace walls on the turbulent flow the k–ε turbulence model was coupled to Wolfshtein's [33], k–l turbulence model in the vicinity of the furnace wall. The gas phase, non-premixed combustion process was modelled by assuming fast chemical reaction via the conserved scalar/prescribed probability density function (p.d.f.) approach using the laminar flamelet concept. A two-parameter, β-p.d.f. was used, with the form of this p.d.f. being specified in terms of the mean and variance of mixture fraction obtained from solution of modelled transport equations. To take account of the heat loss mechanisms the mean temperature was calculated from a transport equation for specific enthalpy. The radiation heat loss from the gas phase was calculated using the optically thin limit [34],

$$S_h = -4K_a(\sigma T^4 - \sigma T_{wall}^4) \tag{11}$$

where the grey absorption coefficient was adjusted to reproduce the temperature field in the main body of the furnace. Note the adjustment of the mean specific enthalpy field to achieve a realistic representation of the mean temperature field is justified as the focus of the paper is the evaluation of flame emission models given as accurate a representation of the flow fields as possible. Soot was modelled using a two-equation approach based on transport equations for soot mass fraction and particle number density [2].

Solution of the transport equations was achieved using a finite-volume technique based on the pressure correction algorithm. The flow field parameters necessary to calculate radiation heat transfer, such as the mean temperature field, were approximated on the finite-volume mesh by taking each control volume to be homogeneous. Further details of the models and numerical solution methods employed, and the flow field results obtained, may be found elsewhere [2,3].

The computational mesh used to calculate the heat transfer fields for the furnace was 2D axisymmetric and consisted of three body fitted blocks: the burner zone (22×20 control volumes), the body of the furnace (62×140) and downstream of the furnace (22×20), see Fig. 3. As this is a closed environment, unlike the free jet fires considered later, heat transfer from the walls of the furnace must be considered. This principally means convection heat transfer to the wall; conduction through the wall and radiation heat flux incident to and reflected from the wall must be included in the model. To account for these processes the wall boundary condition at each wall cell defined by the computational mesh was prescribed as a heat balance

$$q_{CD} = q_{CV} + q_{R,-} - q_{R,+} \tag{12}$$

$$q_{R,-} = \int_{\Delta\Omega} I_{w,-} \cos\theta \, d\Omega \tag{13}$$

$$q_{R,+} = (1 - \varepsilon_w) q_{R,-} + \varepsilon_w \sigma T_w^4 \tag{14}$$

$$q_{CD} = \frac{k_w}{\Delta_w}(T_w - T_{water}) = h_{CD}(T_w - T_{water}) \tag{15}$$

where q_{CD} is the conduction heat transfer through the wall, q_{CV} is the convection heat transfer to the wall and $q_{R,-}$ is the incident radiation heat flux. The incident flux integral is evaluated using a piece-wise constant quadrature in the angle of incidence (θ) and the angle of rotation (φ),

$$q_{R,-} = \sum_{i=1}^{N_\theta} \sum_{j=1}^{N_\varphi} I_{w,-}(\theta_i, \varphi_j) \cos\theta_i \sin\theta_i \sin\Delta\theta\Delta\varphi \tag{16}$$

Other symbols are defined in the nomenclature. Therefore, given the wall emissivity, the convection heat flux and the conduction heat transfer coefficient (12), is a quartic equation in wall temperature that can be solved using any standard numerical technique [35]. The wall emissivity was taken to be 0.8 as recommended by Wu and Fricker [30], and the convection heat flux was prescribed using measured data [30]. The total heat flux distribution was found to be insensitive to the conduction heat transfer coefficient provided values approaching an adiabatic wall were not prescribed. In the furnace simulation discussed further below the conduction heat transfer coefficient was prescribed using thermal conductivities typical of mild steel.

As the walls of the furnace were taken to be grey and total flux boundary conditions prescribed, the discrete transfer method was used iteratively, requiring the incident radiative flux to be 'guessed' and corrected until convergence was achieved. In the present study the incident flux field was initially set to zero and the relative difference between the old and the new incident flux used to measure convergence. A relative difference of less

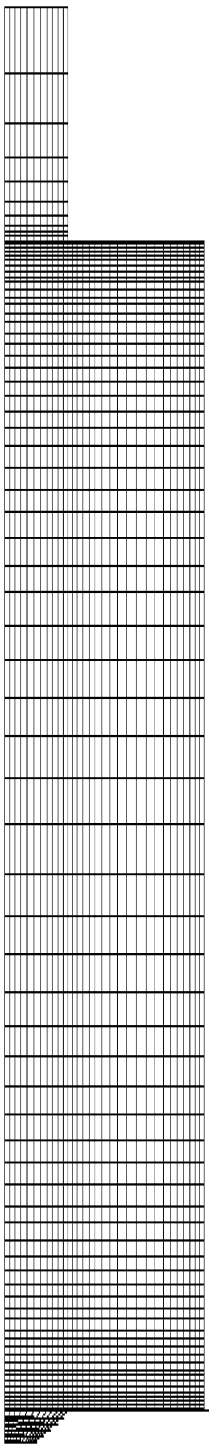

Fig. 3. Finite-volume mesh used for the simulation of Wu and Fricker's flame tube experiment.

than 5% in the change in the incident flux distribution was taken to be the convergence criteria.

In the results given below, predictions of radiation transfer were obtained using mean flow properties, i.e. the influence of turbulence-radiation interactions was ignored. These effects are, however, anticipated to be small in all of the combustion systems considered [2,15].

5.2. Laboratory-scale jet flame

Details of this experiment were given above; in this section the mathematical basis of the flame structure model is presented. The system of transport equations are similar to those discussed in relation to the flame tube simulation. However, there are some simplifications that have been made, exploiting the near parabolic nature of the flow and the fact this is a free jet fire. In laboratory-scale methane jet fires there is insufficient residence time for soot production to be sufficiently large to warrant solving a soot model and there are no walls except at the nozzle so the standard k–ε turbulence model is used without modification. As this is a free jet flame with the dominant flow direction in the vertical direction it is ideally suited to simulate the flow fields using an axisymmetric variant of the boundary layer equations similar to the GENMIX program [36]. This solves the flow equations by marching in the axial co-ordinate direction with a radially expanding non-orthogonal mesh. In the flame structure calculation considered below 40 control volumes in the radial direction were used. In the axial direction the mesh spacing for numerical stability is much smaller than is required to give finite-volume mesh independent predictions of the radiation heat transfer distributions; therefore the thermo-chemical fields required to calculate the radiation heat transfer distribution were represented on a coarsened axial mesh spacing by taking values at every tenth axial station. This gave 125 control volumes in the axial direction. One final simplification is the coupling between the flow fields and the thermal radiation is weak so the radiation heat transfer distribution can be calculated as a post-process to the flame structure simulation. The influence of radiation heat transfer on the flow fields was introduced by modifying the laminar flamelet library to include a fraction of heat radiated as used by Fairweather et al. [2].

5.3. Field-scale jet fire in a cross-wind

The source conditions for the field-scale jet fire give rise to a sonic release that must be accounted for within the numerical methodology used. The approach adopted in the present work was to treat the non-reacting, shock-containing region as an axisymmetric, underexpanded jet [37] and, at the location where the Mach number, M, was 0.6 on the axis, calculated profiles were used as a source specification for either axisymmetric or three-dimensional simulations of the downstream

portions of the flow. A Mach number for the transition of 0.6 was chosen as this represents the point at which compressibility effects become negligible. The main advantage of this solution strategy is that the most appropriate numerical methods can be applied within the two different flow regimes. A further benefit is that the combusting portion of the fire can be treated as an incompressible flow with the density field prescribed by the laminar flamelet library.

For the underexpanded, non-reacting jet simulation in the near field the system of transport equations were discretised over a Cartesian finite-volume mesh superimposed on the domain of interest, with inviscid fluxes approximated using a second-order variant of Godunov's method. The system of algebraic equations derived in this way was then converged by time marching to a steady state. This convergence strategy is efficient for high Mach number flows, and allows grid independent resolution of the shock structures downstream of the release point at a modest computational cost. To further enhance the efficiency of the model, hierarchical adaptive grids were also used, with local grid refinement taking place in regions of steep gradients. A detailed discussion of the numerical solution method employed can be found in Cumber et al. [37].

In the three-dimensional simulations of the combusting portion of the jet fires (where the density field was prescribed via the flamelet) an adaptive, Cartesian mesh was superimposed on the domain of interest. Over each control volume defined by the mesh the system of transport equations was approximated using a finite-volume scheme. In this scheme diffusion terms were represented by a second-order accurate central difference scheme, with advection terms represented using a total variation-diminishing version of the QUICK scheme [37].

In all the computations performed a sufficiently large number of grid nodes were used to ensure that the results presented below were effectively free of numerical error. For example the full three-dimensional simulations employed up to $265k$ nodes (equivalent to 56% of an $x \times y \times z = 112 \times 88 \times 48$ mesh). These values compare favourably with the number of nodes that would be required to achieve equivalent results using a non-adaptive meshing strategy, i.e. $473k$ nodes. Further details of the computation can be found in [3].

6. Results and discussion

6.1. Idealised one-dimensional test case

In evaluating the various participating media models used in conjunction with the discrete transfer method, it is first useful to consider an idealised, one-dimensional situation representative of the non-homogeneous paths encountered in flames and fires. The temperature and mass fraction profiles are given in Fig. 1.

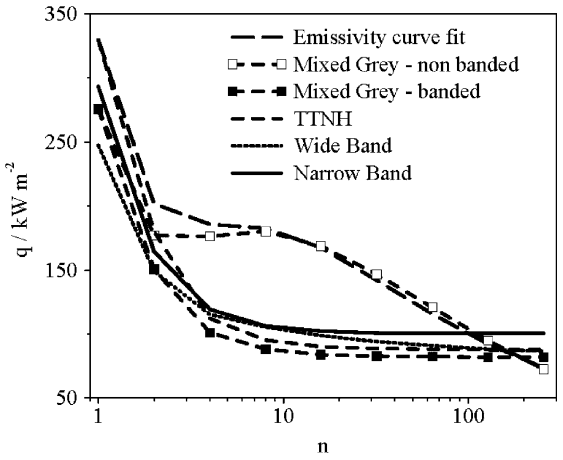

Fig. 4. Variation of received flux with increasing numbers of control volumes for the one-dimensional test case.

Fig. 4 gives results derived from the various models for the profiles of Fig. 1. In obtaining these predictions, the profiles were represented by a number of equal width, homogeneous cells, and the discrete transfer method applied to the one-dimensional "slab" like control volumes constructed. A total of eight rays were used for each calculation, this number of rays having been found to give converged predictions of received heat flux. This approach was employed in order to determine received fluxes rather than the less meaningful radiative intensities that would be derived from strictly one-dimensional computations, i.e. no direction cosine dependence. Results were obtained by doubling the number of control volumes (the abscissa of Fig. 4) used to represent the non-homogeneous profiles from 1 to 256, thereby improving the representation of inhomogeneities along the line-of-sight.

Results derived using the banded version of the mixed grey gas model, the TTNH model, and the wide and narrow band approaches all converge to constant values with increasing numbers of control volumes. This behaviour is essential if reliable predictions of radiation heat transfer are to be obtained in computational fluid dynamic calculations. Once the non-homogeneous profiles along a line of sight are approximated to a sufficient level of accuracy by the finite-volume mesh representation of the relevant flow fields, integration of the radiation transfer equation must return a radiant intensity value independent of further refinement of the finite-volume mesh.

Predictions derived using the grey gas assumption and Modak's [21] emissivity curve fits and the non-banded, mixed grey gas approaches are similar. They do not converge to constant values, with radiation fluxes

decreasing dramatically as the representation of the non-homogeneous path is refined. Similar computations performed for homogeneous mixtures but not reported here also demonstrated that predicted fluxes increase continuously with increasing numbers of control volumes. This occurs since in using these techniques with the recurrence relation of the discrete transfer method a mean absorption coefficient, obtained from the local emissivity, must be specified for each control volume. As path length is reduced however, the mean absorption coefficient obtained increases, and does not tend to zero. This in turn implies that as the computational mesh is refined the sensitivity of the predicted intensity field (or fluxes) to local path length increases. In the discussion of non-convergence of the predicted heat flux using the grey gas approach combined with the discrete transfer method, the important issue is that when the grey gas absorption coefficient is linked to a length scale comparable to the control volume size, such as the length of the ray segment in the control volume, then mesh independent predictions are not possible and this is true whatever the underlying radiation solution algorithm. It could be argued that this issue does not arise if a single length scale is used throughout the computational domain based on a dimension of the combusting flow, but this can be difficult to specify rigorously. An additional argument against the single length scale approach is it goes against the underlying philosophy of CFD simulation. This convergence problem, caused by the assumption of grey gas behaviour, is well known in the radiation modelling community, but applications of this type of methodology, in conjunction with numerical solutions to the fluid flow equations, still appear in the literature [7] being an example. Edwards [14] describes this as "the grey gas myth" in relation to a single absorption coefficient representing the detailed line structure in the spectral dimension for emission from participating species. To aid appreciation of why the grey gas approximation breaks down at small path lengths, consider a homogeneous slab at a temperature T and thickness l. Considering the spectrally integrated intensity of a ray with a normal orientation to the slab the intensity on exit is

$$I(l) = \varepsilon_T(l)\sigma\frac{T^4}{\pi} \tag{17}$$

taking the intensity on entry to the slab as zero. Subdividing the homogeneous slab into two equal volumes the intensity on exit can also be calculated as

$$I(l) = \left(2 - \varepsilon_T\left(\frac{l}{2}\right)\right)\varepsilon_T\left(\frac{l}{2}\right)\sigma\frac{T^4}{\pi} \tag{18}$$

Equating (17) and (18) and simplifying gives the relation,

$$\varepsilon_T(l) = \left(2 - \varepsilon_T\left(\frac{l}{2}\right)\right)\varepsilon_T\left(\frac{l}{2}\right) \tag{19}$$

which in general is not true for total emissivity correlations at small path lengths as this property is sacrificed for agreement with total emissivity data at larger path lengths.

Modak's emissivity curve fits were never intended for use in a CFD framework, however there ease of implementation and short run-time make them an attractive option for a non-expert in thermal radiation modelling as radiation heat transfer can thereby be incorporated in combustion simulations with minimal effort and little computational overhead. Considering the non-banded mixed grey gas model results, they do not imply that the mixed grey gas model cannot be applied in combustion computations to yield reliable results. The results and conclusions reached here are a function of the way in which these models have been implemented in conjunction with the discrete transfer method. Nevertheless, computations based on the non-banded implementation abound in the literature.

Table 1 gives speed-up factors, relative to run-times of the narrow band approach, for the flame emission models that gave converged results for the one-dimensional test case, with the factors quoted being for received fluxes which varied by less than 2% when the number of control volumes was doubled. As might be anticipated, the run-times of the wide and narrow band approaches far exceed those of the alternative methods due to the intensive nature of detailed spectral calculations. Surprisingly, however, the run-time of the wide band approach was greater than that of the more intensive narrow band model primarily due to the large number of control volumes required to give converged results. This anomalous result was investigated further and found to be due to the wide band model's implementation. When using the spectral version of the wide band

Table 1
Speed-up factors for various flame emission models

Radiation model	One-dimensional test case			Laboratory-scale flame	Field-scale fire		
	n	S	S_{CV}	S_{CV}	N_{Ray}	S	S_{Ray}
Mixed grey-banded	32	309.2	618.4	25.9	416	273.1	278
TTNH	16	142.7	142.7	20.2	465	75.4	85.9
Wide band	128	0.6	4.8	2.8	423	4.1	4.3
Narrow band	16	1	1	1	408	1	1

model rather than the grey band version, Edward's [14] recommends increasing the band width parameter (ω) by 20%. Cumber et al. [15] subsequently suggested increasing the band width parameter by 20% except in the linear growth region ($\tau_H < \eta < 1$). This proposal has a theoretical basis and gives marginally more accurate predictions of intensity distribution for the cases considered, see [15] for details. However, the more accurate implementation of the model has a major disadvantage when applied to the one-dimensional test case where the computational mesh is successively refined as the step change in the band width parameter makes the predicted flux overly sensitive in the case of coarse meshes. The mixed grey gas, TTNH and narrow band approaches all require relatively small numbers of control volumes to represent the non-homogeneous profiles to a sufficient degree of accuracy, with the former methods giving speed-up factors, respectively, of more than 300 and almost 150 relative to the narrow band model.

It is interesting to note that the two flame emission models based on the integral form of the equation of radiation heat transfer, the TTNH model and the narrow band model are the least sensitive to the resolution of the finite-volume mesh. It could be argued that although band scaling techniques are computationally intensive compared to models based on the differential form of the equation for radiation heat transfer [19], the additional run-time could be balanced to some extent by producing satisfactory incident flux predictions using coarser meshes.

Grosshandler [22], when comparing the computer run-time of the TTNH model and the narrow band model gave an indicative speed-up of between 400 and 600 times compared to 143 in this study. The difference is the overhead associated with the ray trace necessary to evaluate the radiation flux in this study rather than Grosshandler's practice of comparing run-times for evaluating intensities along single rays. It is possible to perform the ray trace once and store the information to reduce the overhead of the ray trace [38] where the radiation fields are coupled to the flow fields. However, the stored ray trace represents a large amount of data that limits the size of the problem that can be simulated.

6.2. Flame tube simulation

The idealised case considered so far is instructive but is not representative of how a radiation model would generally be used in practice. In computations of flames and fires, a grid-independent numerical solution for the internal structure of the fire would (at some stage) be made available to the radiation calculation, either as part of a coupled fluid flow-radiation transfer procedure, or with received fluxes determined by post-processing. In either case, once the ray-tracing element of the discrete transfer method has been performed, the number of homogeneous cells used to represent a non-homogeneous path through the fire would be fixed, with the path length through each homogeneous control volume also determined by the ray tracing algorithm.

For the remainder of this article the flame emission models that could not achieve a mesh independent heat flux in the one-dimensional test case will not be considered further and attention will be focused on the remaining four models; these are the banded implementation of the mixed grey gas model, Grosshandler's TTNH model, the wide band model and the narrow band model.

This simulation is of interest as it provides the opportunity to assess the flame emission models in a scenario where soot emission is a significant component of the energy transfer budget. The influence of soot on radiation heat transfer has been considered previously for the mixed grey gas model but only for idealised one-dimensional profiles [39].

The mean temperature field was adjusted by introducing a radiation loss term in the transport equation for specific enthalpy based on the optically thin limit as discussed above. This is valid in the burner region as the radiation heat loss is dominated by banded radiation from participating species. Further downstream where significant soot concentrations are present this may not be valid, although the predicted homogeneity of the temperature field is maintained. The predicted and measured radial temperature distributions at two downstream locations are presented in Fig. 5. Close to the burner, near the axis, the agreement is not particularly good, but improves with increasing distance from the axis, and further downstream the agreement is much improved. The homogeneity of the temperature field is clearly demonstrated in both the experiment and the simulation.

Fig. 6 shows contour maps for the temperature, soot volume fraction, CO_2 and H_2O mass fraction fields. In the temperature field eight temperature contour values are plotted from 300 to 1700 K with a spacing of 200 K. In the soot volume fraction field eight equi-logarithmic contours are plotted. In the final two contour maps ten equi-spaced values are plotted between the predicted minimum and maximum values. The values of each individual contour can be inferred from Fig. 7. Fig. 7 shows the predicted temperature, soot volume fraction and the CO_2 and H_2O mass fractions on the centre-line of the furnace. The flow fields in the furnace can be characterised into two zones, the burner zone and the far field zone. In the burner zone gradients are steep and radiation heat transfer is primarily emission from participating species. Further downstream, soot concentrations are significant and the temperature and participating gas species fields are smooth, being well approximated to be homogeneous.

As discussed above, for grey walled enclosures and where radiation boundary conditions are prescribed

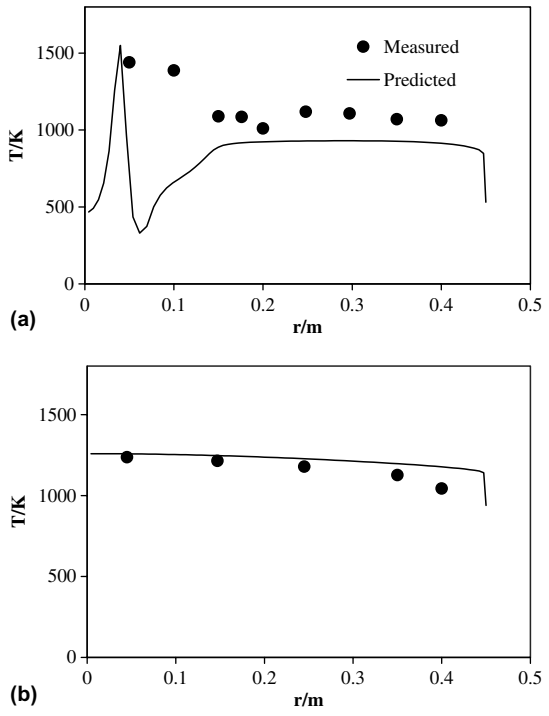

Fig. 5. Radial temperature distributions at (a) $z = 0.231$ m and (b) $z = 3.831$ m.

using a heat balance the radiation solver is iterative. A relative difference of 5% between the old and new incident flux distributions during the iterative cycle typically required three iterations of the discrete transfer method for all flame radiation models except the mixed grey gas model, which required four iterations. To evaluate the incident radiation flux the radiation intensity field was found to be sufficiently homogeneous that only 12 rays per wall cell were required to evaluate a ray-independent incident radiation heat flux distribution on the furnace wall. Increasing the number of rays to 48 rays per wall cell changed the predicted incident flux by less than 2%. This is in sharp contrast to the jet fire radiation fields discussed below where significantly more rays were required.

Fig. 8 shows the predicted total heat flux distributions together with the measured total heat flux. The measured heat flux distribution is included to show that all model predictions qualitatively agree with the measurements. The narrow band model quantitatively predicts the maximum total heat flux, but like all of the other models over-predicts the measured heat flux downstream of the peak value. When considering the 'accuracy' of the respective flame emission models, the closeness of agreement to the measurements relies on both the basis of the flame radiation model and the radiation model inputs derived from the fluid flow simulation. For example it is difficult to validate the soot model used in the furnace simulation as no soot concentration measurements are available for comparison. If the soot model over-predicted the soot concentration then it would be unreasonable to expect any flame radiation model to predict the wall heat flux distribution. However, taking these discrepancies on board, the narrow band model predictions can be considered the most accurate in the sense that the model has the most sophisticated basis. Therefore, statements about model accuracy for the other flame radiation models can be made by comparing predicted heat flux distributions with the narrow band model predictions.

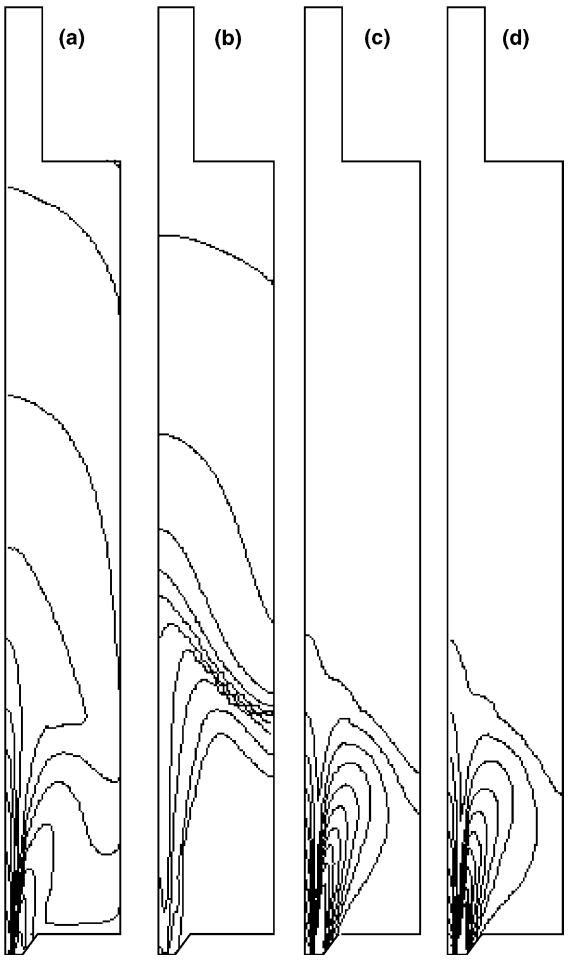

Fig. 6. Contour maps of (a) mean temperature, (b) soot mass fraction, (c) CO_2 mass fraction and (d) H_2O mass fraction.

All models tend to over-predict the total heat flux close to the burner where soot concentrations are low. Further upstream, as the soot levels increase, the mixed grey gas model and the wide band model converge to the narrow band prediction of total heat flux. The TTNH model prediction of total heat flux distribution

over-predicts the narrow band model prediction over the length of the furnace wall. This is further emphasised by factoring out the prescribed convection heat flux distribution in the comparison. Fig. 9 shows the radiation heat flux for all four flame emission models. Overall the mixed grey gas model prediction of radiation heat flux is the closest to the narrow band model prediction except close to the burner. In the burner region all three model predictions of radiation heat flux are significantly larger than the narrow band model prediction. The similarity of the predicted heat flux in the far field of the burner for all four flame emission models suggests that where soot emission is significant the predicted heat flux is insensitive to the model implemented.

The computational cost of each of the models is summarised in Table 2. The speed-up parameter is expressed in terms of the narrow band model run-time. Two speed-up parameters are given for the mixed grey gas model, one is for the simulation as a whole and the other is for a single iteration of the discrete transfer method. The speed-up parameter for a single iteration is possibly more representative of the likely cost of using the mixed grey gas model compared to the narrow band model, as convergence in three or four iterations of the discrete transfer method is a threshold effect. The convergence characteristics for the discrete transfer method were affected by the flame emission model implemented, but not significantly so. Where the radiation model and fluid flow solver are coupled such that the discrete transfer method is called periodically, reasonable estimates of the incident heat flux distributions are available, typi-

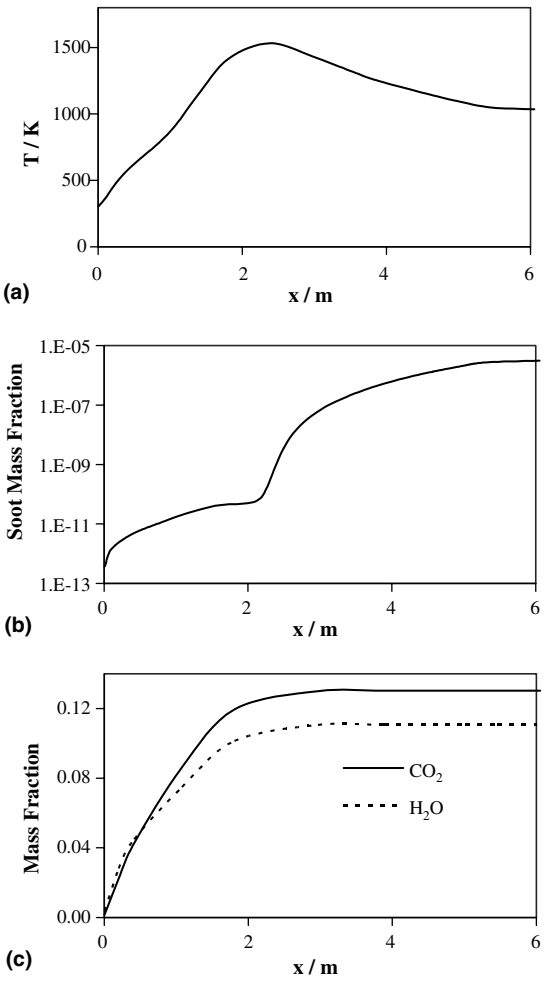

Fig. 7. Axial distribution of (a) mean temperature, (b) mass fraction of soot and (c) mass fraction of CO_2 and H_2O.

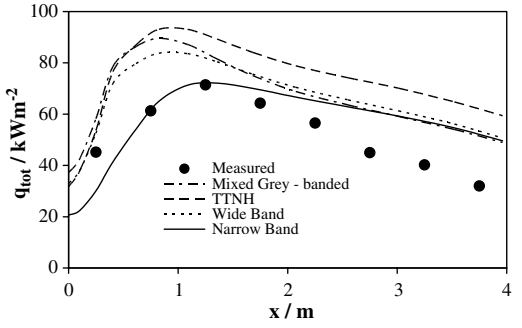

Fig. 8. Total heat flux distribution on the flame tube wall.

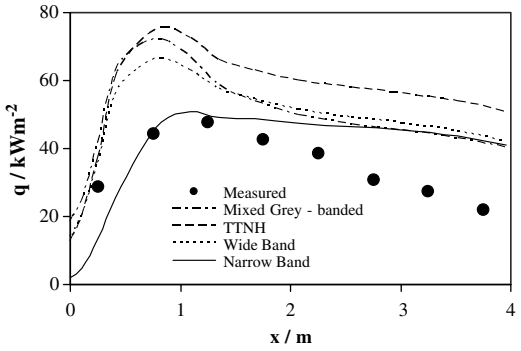

Fig. 9. Radiation heat flux distribution on the flame tube wall.

Table 2
Speed-up parameters for various flame radiation models applied to Wu and Fricker's furnace simulation

Radiation model	S_{CV}	S_{CV} (one iteration)
Mixed grey-banded	164	217
TTNH	76.8	76.8
Wide band	2.9	2.9
Narrow band	1	1

cally reducing the number of iterations of the discrete transfer method to one per call of the radiation model.

6.3. Laboratory-scale jet flame

Numerical calculations using the flame structure models described earlier were made for two flames of widely differing scales. The application of flame emission models to jet fires at these two diverse scales is a severe test of the generality of the respective models. The first is a laboratory-scale methane flame considered by Baillie et al. [31]. In deriving the results for radiation fluxes given below, radiation calculations were performed using the discrete transfer method as a post-process on converged and mesh-independent numerical calculations of the combusting flow fields. For the laboratory-scale flame, use of the discrete transfer method in conjunction with 192 rays per receiver of radiation (radiation heat flux meter) was found to give ray converged values for the fluxes for all receiver locations and flame emission models. A staggered ray distribution [40] was also employed over the hemispherical surface about each receiver in order to improve numerical convergence characteristics and run-times.

Thermal radiation levels about the laboratory-scale jet flame were measured using a radiometer with a 150° field of view and by tracking the radiometer vertically (z) at a horizontal distance of 0.4 m from the release, with its normal pointing towards the flame, and horizontally (r) at the height of the pipe exit with its normal pointing vertically upwards. The results obtained are shown, respectively, in Figs. 10 and 11.

Figs. 10 and 11 show results for the laboratory-scale flame obtained using the four flame emission models that yielded converged predictions in conjunction with the discrete transfer method, with Table 1 showing model run-times, again in terms of a speed-up factor relative to results obtained using the narrow band approach. Values of S given in Table 1 are averages over all receiver locations. The level of agreement between each of the four models and the experimental data displayed in the latter figures is satisfactory, with all the models being generally within 20% of observations. Agreement between predictions of the various models and the data is, however, dependent to some degree on the accuracy of the mathematical basis of the flame structure model given that the numerical error is negligible, because of this these results are of limited use in assessing the relative accuracy of the various flame emission models. A more meaningful comparison is between predictions of the various models and results derived using the more accurate narrow band approach, which reveals that fluxes obtained using the banded grey gas and wide band models are within 13% of the narrow band results, whilst those of the TTNH approach are within 22%. This level of performance may be considered adequate for most flame calculations. The results of Table 1 also demonstrate that in applying these models to real flame calculations, for this flame at least, the speed-up factors realised for the idealised, one-dimensional test case are not achieved in practice. In particular, the run-times associated with the banded version of the mixed grey gas model and the TTNH approach are now an order of magnitude less than those achieved for the latter case. In addition, run-times of the wide band model are now almost three times faster than those of the narrow band approach, primarily due to the fact that, compared to the one-dimensional test case, the number of homogeneous elements used to represent any non-homogeneous path has been dramatically reduced.

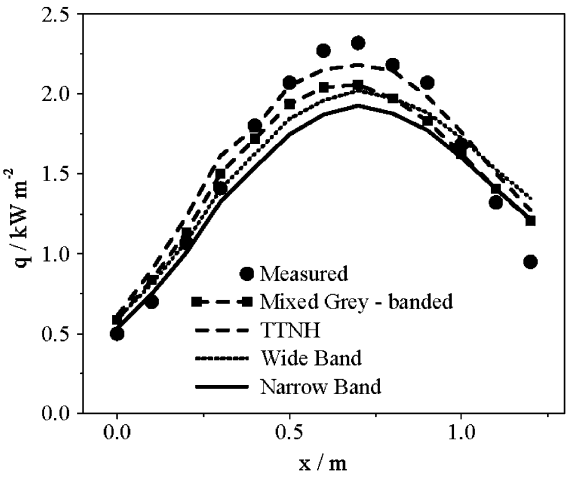

Fig. 10. Variation of radiation fluxes with vertical distance for the laboratory-scale flame.

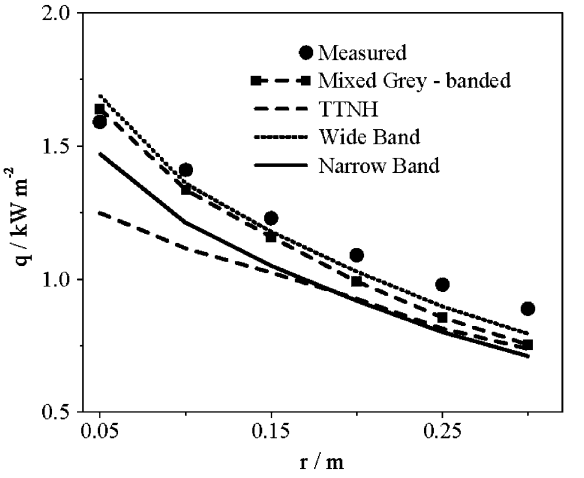

Fig. 11. Variation of radiation fluxes with horizontal distance for the laboratory-scale flame.

6.4. Field-scale jet fire in a cross-wind

Fig. 12(a) shows the predicted temperature field on the symmetry plane showing the influence of the cross-wind on the flame structure. Fig. 12(b) gives the predicted temperature field on a number of horizontal planes through the fire with increasing height, where the influence of a horseshoe vortex within the flow on the flame structure can be seen. Radiation measurements about the fire were made using radiometers that were positioned downwind (x) with their normals orientated towards the fire in order to maximise received radiation fluxes. The received fluxes obtained are given in Fig. 13.

For the field-scale fire, a ray adaption technique was used to improve model run-times because of the remote location of receivers and the domination of the radiation field by a relatively small hot emitting volume which would require a large number of rays. This is a classic example of the ray effect [41]. Therefore different numbers of rays were employed in a hierarchal adaptive ray distribution in conjunction with each flame emission model, although, as will be seen later, the total number of rays used was similar in each case. Details of the adaptive ray mesh algorithm can be found in [40,42].

The results displayed in Fig. 13 for the field-scale fire tend to confirm the conclusions reached above for model accuracy. In particular, predictions of the banded grey gas and wide band models are within 10% of narrow band model results, although the TTNH approach consistently over-predicts the latter model by between 80% and 90%. In real terms, however, this is only a problem

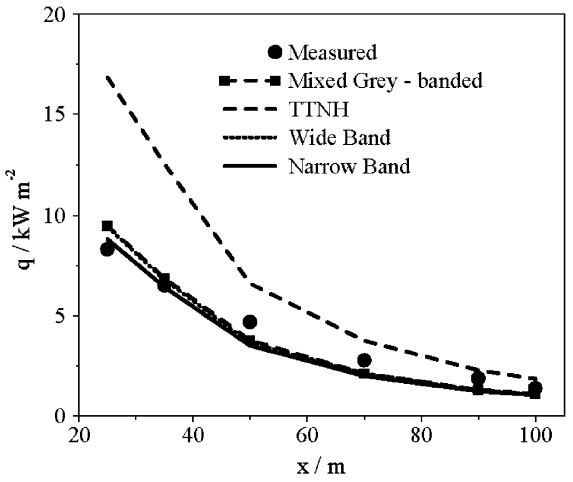

Fig. 13. Variation of radiation fluxes downwind of the field-scale fire.

close to the fire, as displayed in Fig. 13. Compared to the laboratory-scale flame, the run-times of the various models, given in Table 1, are now more in line with those obtained for the one-dimensional test case, with the TTNH and mixed grey approaches being, respectively, one and two orders of magnitude faster than the narrow band model.

The differences in model run-times exhibited in the results of Table 1 may be attributed to the increasing dominance of the ray-tracing algorithm within the discrete transfer method in increasingly complex geometric

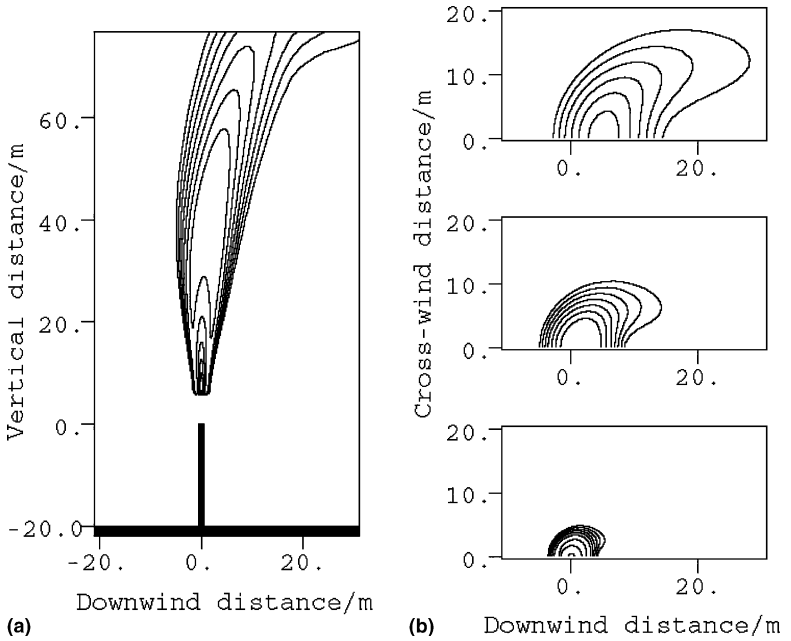

Fig. 12. Predicted mean temperature field for a field-scale jet fire (3.2 GW), (a) symmetry plane and (b) three horizontal planes.

configurations. For the field-scale fire, ray tracing was performed through a three-dimensional, Cartesian mesh. These computations are simpler than the laboratory-scale jet flame ray trace calculations but more complex than the ray trace for rays in a one-dimensional finite-volume mesh, hence the difference in speed-up parameter between different simulations. For the laboratory-scale flame, the ray-tracing algorithm was used in conjunction with an axisymmetric finite-volume mesh that expanded in the downstream and cross-stream directions. As a consequence the ray trace was a significant computational overhead for all of the radiation flux computations, and dramatically reduced the speed-up parameter. The speed-up parameter results for the flame tube simulation are bracketed by the field-scale fire and the laboratory-scale flame speed-up results. This is due to the nature of the finite-volume mesh used in the flame tube simulation as only the burner zone block used a non-orthogonal expanding mesh similar to the mesh used for the jet fire model, whereas the other two blocks were axisymmetric orthogonal blocks that resembled Cartesian meshes in the r–z plane. The relevant speed-up parameters that must be considered are the speed-up per control volume (one-dimensional test case and the laboratory-scale jet flame), and the speed-up parameter per ray (field-scale jet fire). Different flame emission models are affected to a different degree by the changes in ray trace complexity. For example, considering the banded mixed grey gas model applied to the one-dimensional test case, a speed-up per control volume of almost 620 decreases by more than an order of magnitude to 25.9 for the laboratory-scale jet flame, a reduction of 96%. In contrast, the same simulations for the wide band model show that the speed-up parameter per control volume changes from 4.8 to 2.8, a reduction of 42%.

A limited number of computations were also performed using the temperature correction factor to the transmittance determined within the TTNH model suggested by Grosshandler [22]. In all cases, the incorporation of this factor significantly reduced agreement between the TTNH model results and those obtained using the narrow band approach. Further work to improve the applicability of this factor to the conditions encountered in computational fluid dynamic calculations of fires would be useful.

7. Conclusions

Comparing the performance of the flame emission models for the jet flames/fires and the flame tube simulation, broadly speaking the speed-up characteristics are consistent and any differences are associated with the different finite-volume meshes used. In previous comparisons of the wide band model and the narrow band model, typically the wide band model is shown to be an order of magnitude faster with predictions of integrated intensity, and hence radiation flux, within 10% of the narrow band prediction. The disappointing speed-up of the wide band model is due to its use of an expression for the spectral transmissivity rather than the grey band assumption implemented by Edwards, necessary for use in a CFD framework. This means the spectral intensity distribution must be evaluated using a numerical quadrature rather than a relatively simple evaluation of a piecewise constant spectral distribution. This problem could be partially resolved by implementing the adaptive quadrature technique used successfully by Cumber [40,42] to evaluate the incident flux integral. Another factor is that the ray trace is included in the run-time of both models, tending to reduce the speed-up factor for the wide band model.

One conclusion from this study is the implementation of simple participating media models within the discrete transfer method, based on the assumption of grey gas behaviour is not appropriate for non-homogeneous systems as radiation fluxes predicted using this approach do not converge as the representation of a non-homogeneous path is refined. In general, the banded grey gas, TTNH, wide and narrow band models yield satisfactory results for flame and fire applications, with an adequate level of agreement between the various models, and with experimental data.

This article highlights the significant overhead of the ray trace used in the discrete transfer method, and in particular how the type of finite-volume mesh employed to represent the flame structure modifies the run-time of any radiation model implemented. For computations of fires obtained in conjunction with Cartesian meshes, the TTNH and banded grey gas models give speed-up factors, respectively, of one and two orders of magnitude relative to the wide and narrow band approaches. The performance of all models relative to the narrow band approach is, however, dramatically reduced when more complex, non-Cartesian meshes are employed.

Results for the idealised test case indicate that only a relatively small number of homogeneous cells are required by some models to represent a non-homogeneous profile. This suggests that radiation calculations for fires, depending on the flame emission model, could be performed on meshes that are coarser than those generally used for the fluid dynamic computations. Use of the wide band model should be treated with some caution due to the large number of control volumes required to give converged results. This situation can be improved with some thought given to the computer implementation of the model in the context of a CFD framework, or through use of wide band scaling techniques. However, wide band-scaling techniques are likely to introduce a significant computational overhead

even though fewer control volumes may be required to achieve finite-volume mesh independent predictions.

References

[1] M. Caulfield, D.K. Cook, P. Docherty, M. Fairweather, An integral model of turbulent jets in a cross-flow. Part 2—Fires, Trans IChemE, Part B: Process Saf. Environ. Prot. 71 (1993) 243–251.

[2] M. Fairweather, W.P. Jones, R.P. Lindstedt, Predictions of radiative heat transfer from a turbulent reacting jet in a cross-wind, Combust. Flame 89 (1992) 45–63.

[3] R.P. Cleaver, P.S. Cumber, M. Fairweather, Predictions of sonic jet fires, Combust. Flame 132 (2003) 463–474.

[4] F.C. Lockwood, N.G. Shah, A new radiation solution method for incorporation in general combustion prediction procedures, in: Eighteenth Symposium (International) on Combustion, The Combustion Institute, Pittsburgh, 1981, pp. 1405–1414.

[5] Y.R. Sivathanu, J.P. Gore, Coupled radiation and soot kinetics interaction in laminar acetylene/air diffusion flames, Combust. Flame 97 (1994) 161–172.

[6] J.S. Truelove, A mixed grey gas model for flame radiation, AERE-R8494, UKAEA, Harwell, 1976.

[7] F.C. Lockwood, W.M. Malalasekera, Fire computation: the flashover phenomenonTwenty Second Symposium (International) on Combustion, The Combustion Institute, Pittsburgh, 1988, pp. 1319–1328.

[8] M.J. Lewis, P.A. Rubini, J.B. Moss, Field modelling of non-charring flame spread, in: Proceedings of the 6th Fire Safety Science Symposium, Poitier, France, 1999, pp. 683–694.

[9] D.N. Trivic, Modelling of 3D non-gray gases radiation by coupling the finite volume method with weighted sum of gray gases model, Int. J. Heat Mass Transfer 47 (2004) 1367–1382.

[10] A. Soufiani, E. Djavdan, A comparison between weighted sum of gray gases and statistical narrow-band radiation models for combustion applications, Combust. Flame 97 (1994) 240–250.

[11] S.M. Jeng, M.C. Lai, G.M. Faeth, Nonluminous radiation in turbulent buoyant axisymmetric flames, Combust. Sci. Technol. 40 (1984) 41–53.

[12] D.K. Edwards, W.A. Menard, Comparison of models for correlation of total band absorption, Appl. Opt. 3 (1964) 62–626.

[13] D.K. Edwards, A. Balakrishnan, Thermal radiation by combustion gases, Int. J. Heat Mass Transfer 16 (1973) 25–40.

[14] D.K. Edwards, Molecular gas band radiation, in: T.F. Irvine, J.P. Hartnett (Eds.), Advances in Heat Transfer, vol. 12, Academic Press, New York, 1976, pp. 115–193.

[15] P.S. Cumber, M. Fairweather, S. Ledin, Application of wide band radiation models to non-homogeneous combustion systems, Int. J. Heat Mass Transfer 41 (1998) 1573–1584.

[16] J.G. Marakis, Application of narrow and wide band models for radiative transfer in planar media, Int. J. Heat Mass Transfer 44 (2001) 131–142.

[17] W. Malkmus, Random Lorentz band model with exponential-tailed S^{-1} line-intensity distribution function, J. Opt. Soc. Am. 57 (1967) 323–329.

[18] T.K. Kim, J.A. Menart, H.S. Lee, Non-gray radiative gas analyses using the *S–N* discrete ordinates method, J. Heat Transfer 113 (1991) 946–952.

[19] J. Strohle, P.J. Coelho, On the application of the exponential wide band model to the calculation of radiative heat transfer in one and two dimensional enclosures, Int. J. Heat Mass Transfer 45 (2002) 2129–2139.

[20] N. Lallemant, A. Sayre, R. Weber, Evaluation of emissivity correlations for H_2O–CO_2–N_2/air mixtures and coupling with solution methods of radiative transfer equations, Progr. Energy Combust. Sci. 22 (1997) 543–574.

[21] A.T. Modak, Radiation from products of combustion, Fire Res. 1 (1978) 339–361.

[22] W.L. Grosshandler, Radiative heat transfer in non-homogeneous gases: a simplified approach, Int. J. Heat Mass Transfer 23 (1980) 1447–1459.

[23] W.L. Grosshandler, H.D. Nguyen, Application of the total transmittance non-homogeneous radiation model to methane combustion, J. Heat Transfer 107 (1985) 445–450.

[24] M.F. Modest, The weighted sum of gray-gases model for arbitrary solution methods in radiative transfer, J. Heat Transfer 113 (1991) 650–656.

[25] W.L. Grosshandler, A.T. Modak, Radiation from non-homogeneous combustion products, in: Eighteenth Symposium (International) on Combustion, The Combustion Institute, Pittsburgh, 1981, pp. 601–609.

[26] R.M. Goody, Atmospheric Radiation I: Theoretical Basis, Clarendon Press, Oxford, 1964.

[27] W.H. Dalzell, A.F. Sarofim, Optical constants of soot and their application to heat flux calculations, J. Heat Transfer 91 (1969) 100–104.

[28] Z. Yan, G. Holmstedt, Fast, narrow-band computer model for radiation calculations, Numer. Heat Transfer, Part B 31 (1997) 61–71.

[29] T. Okamoto, T. Mutou, T. Takagi, Approach for incorporating narrow band non-uniformity into non-gray analysis of radiative heat transfer in non-isothermal and non-homogeneous gas fields, Int. J. Heat Mass Transfer 44 (2001) 4147–4156.

[30] H.L. Wu, N. Fricker, The characteristics of swirl-stabilized natural gas flames, Part 2: The behaviour of swirling jet flames in a narrow cylindrical furnace, J. Inst. Fuel 49 (1976) 144–151.

[31] S. Baillie, M. Caulfield, D.K. Cook, P. Docherty, A phenomenological model for predicting the thermal loading to a cylindrical vessel impacted by high pressure natural gas jet fires, Trans IChemE, Part B: Process Saf. Environ. Prot. 76 (1998) 3–13.

[32] D.K. Cook, P.S. Cumber, M. Fairweather, F. Shemirani, Modelling free and impacting underexpanded jet fires, in: IChemE Symposium Series, No. 141, The Institution of Chemical Engineers, Rugby, 1997, pp. 127–138.

[33] M. Wolfshtein, The velocity and temperature distribution in one-dimensional flow with turbulence augmentation and pressure gradient, Int. J. Heat Mass Transfer 2969 (12) 301–312.

[34] R. Siegel, J.R. Howell, Thermal Radiation Heat Transfer, third ed., Hemisphere Publishing Corporation, 1992.

[35] W.H. Press, S.A. Teukolsky, W.T. Vetterling, B.P. Flannery, Numerical Recipes in Fortran 77, second ed., Cambridge University Press, 1992.
[36] D.B. Spalding, GENMIX: A General Computer Program for Two-dimensional Parabolic Phenomena, Pergamon Press, Oxford, 1977.
[37] P.S. Cumber, M. Fairweather, S.A.E.G. Falle, J.R. Giddings, Predictions of the structure of turbulent, moderately underexpanded jets, J. Fluid Eng. ASME 116 (1994) 707–713.
[38] P.S. Cumber, Improvements to the discrete transfer method of calculating radiative heat transfer, Int. J. Heat Mass Transfer 38 (1995) 2251–2258.
[39] N.W. Bresloff, The influence of soot loading on weighted sum of grey gases solutions to the radiative transfer equation across mixtures of gases and soot, Int. J. Heat Mass Transfer 42 (1999) 3469–3480.
[40] P.S. Cumber, Ray effect mitigation in jet fire radiation modelling, Int. J. Heat Mass Transfer 43 (2000) 935–943.
[41] J.C. Chai, S.L. HaeOk, S.V. Patankar, Ray effect and false scattering in the discrete ordinates method, Numer. Heat Transfer, Part B 24 (1993) 373–389.
[42] P.S. Cumber, Application of adaptive quadrature to fire radiation modelling, J. Heat Transfer, ASME 121 (1999) 203–204.